Numerical Modelling of Thermal Spray Systems

C. Amon, F. Prinz, K. Schmaltz

EDRC 24-106-93

NUMERICAL MODELLING OF THERMAL SPRAY SYSTEMS

Cristina H. Amon, Fritz Prinz
and Kevin Schmaltz
Department of Mechanical Engineering

Abstract

The purpose of this paper is to present a brief overview of the MD* thermal spray process, review the current existing models of heat transfer and fluid mechanics relevant to this process, outline a simplified thermal model implemented together with the results, and discuss the activities required for the implementation and verification of an accurate temperature model of the MD* thermal spray process. The thermal model involves a mixed Lagrangian/explicit Eulerian algorithm to track the solidification for the time-dependent, one-dimensional heat equation. The effect of operating parameters (droplet/substrate temperatures, droplet size, etc.) on temperature distribution and remelting thickness is predicted. Furthermore, the motivation behind the desire for accurate spray temperature prediction of the ongoing Navigator project will be discussed.

NUMERICAL MODELLING OF THERMAL SPRAY SYSTEMS

Overview

The original uses of thermal spray techniques involved the application of thin films, either for the corrosion resistance or thermal properties of the film material. The thermal spray process also offers a novel manufacturing technique with advantages over more conventional forming methods (i.e., casting and machining) by virtue of its ability to rapidly fabricate a near net-shape structure. The spray process developed at Carnegie Mellon is known as MD* (Weiss, et al. 1992). In this process, an object (monolith) is built up by the spraying of successive layers of material, while the monolith's shape is maintained either through the use of spray masks for each deposition layer or by machining after each sprayed layer. This process permits the manufacturing of complex geometric structures and the selection of varied material deposition for composite and laminate structures that would either be difficult or impossible to create using traditional methods. Additionally, this method will permit rapid prototyping. A further benefit is the feasibility of integrating electronic and mechanical assemblies in which the electronic components are embedded within the sprayed structure and the interconnecting wiring are generated via the spray process.

The goal of the Navigator project is to manufacture a wearable computer capable of providing specific navigating information to the user. The computer interface is either voice or mouse activated, and a small display screen is provided near the user's eye. Spray manufacturing has been selected for the Navigator, among other reasons, for its flexibillty in packaging the electronics as well as its ability to provlde any necessary configurations dictated by heat removal requirements.

There are three methods of thermal spraying under consideration for the Navigator project: electric arc, plasma, and weld-based spray. With the electric arc method the deposition material is continuously fed into the spraying apparatus in wire form. An arcing current is passed through the material to be sprayed, melting it, while a gas propels the molten material to the substrate where solidification takes place (Gerdeman and Hecht, 1972).

The plasma spray process, which was originally used as a means of providing intense heat for experimental purposes, generates the heat necessary to melt the deposition material by passing an inert gas (usually argon) across two electrodes. Electrons from the gas molecules are stripped and accelerated creating a plasma that is far above the melting point of any material (10,000+ °K). The material to be sprayed, which is typically in powder form, is then fed into the discharge of the plasma gun and propelled by the inert gas onto a substrate (Gerdeman and Hecht, 1972).

The third process, weld-based spray, employs a process similar to conventional welding, where the material to be deposited is originally in wire form. Unlike traditional welding, the wire is elevated away from the substrate in order to protect the deposited layers from the heat generated by the melting process, although high droplet temperatures are created.

While the plasma process has the highest gas nozzle temperatures (in the range of 5,000+ °C), the actual droplet temperatures existing at impact are comparable to the electric arc process. This is due to the fact that while the rate of plasma to droplet energy transfer is greater for the plasma process, it is the ensuing heat transfer to atmosphere occurring during the droplets[9] flight to the sprayed surface that is the dominant factor. For both the plasma and arc

processes the droplets are small (on the order of hundreds of 100 microns) and the heat transfer cools the droplets to near melting point conditions. With the welding process the droplets are larger (thousands of microns range) than for the previous processes. Because of the greater droplet volume to surface ratio for this process the release of droplet heat to the atmosphere is less complete at impact and the temperature of these impinging droplets is consequently greater.

Both the electric arc and the plasma spray methods result in droplets that are nearly at their melting points at impact (either above or below). The welding method is the sole process of the three that generates liquid droplet temperatures significantly above the melting point. The welding and electric arc methods are restricted to spraying metals, while the plasma method could also be used to apply plastics or ceramics.

The results for the different deposition processes can vary considerably from one method to the next. In particular the plasma spray process, with its considerable nozzle temperature, will require consideration of radiation heat transfer taking place from the nozzle to the deposit surface. The welding spray process introduces the most heat to the substrate because of the relatively large droplet sizes and temperatures. With this process the solidified substrate may be remelted by the impinging droplets. This remelting has crucial effects on the quality of the bonding of successive deposition layers, and will be closely examined in the modelling process.

During the process of spraying the electronic wiring within the monolith it will be necessary to ensure that the fabrication temperatures remain below any maximum limit set for the electronic components. This is in opposition to the fact that the quality of the bonding of the successive layers is improved if the

impinging liquid droplets have sufficient energy to slightly remelt to previous layer deposited. The extent of remelting must remain slight in order to maintain the dimensional integrity of the monolith. The motivations for modelling the melting phenomenon are therefore to aid in both the selection of manufacturing process parameters that protect the electronics and optimize the remelting.

The properties of the deposited materials (mechanical, electrical, and thermal) vary depending on the choice of spraying parameters. Beyond the remelting effect, the rate of cooling of the deposited material will also determine its structure, and thereby its material properties. These properties can be significantly different from non-sprayed values for the same material. Modelling of the temperatures that result from different application techniques could allow the more accurate prediction of material properties. With better knowledge of the anticipated properties, modifications to both the spray process and the system configuration could be proposed to maintain optimal operating temperatures for the device.

Existing Thermal Models

Efforts to predict the temperatures generated in spray processes have been performed by several researchers. The spray processes considered have involved gas-propelled, plasma or electric arc heat methods. The materials sprayed have usually been metals (or alloys) sprayed in thin films onto metal substrates for the purpose of surface protection.

With previous models (Pawlowski et al.[9] 1981; Pawlowski, 1982) the plasma spray process is modelled using both an analytical and a finite difference approach, considering only one-dimensional heat transfer. The analytical

method uses simplifying assumptions regarding the heat transfer across deposit layer interfaces. Linear temperature profiles are assumed across the deposition layer, and there is no calculation of the melting front location. **Instead,** both models treat the latent heat released during solidification as a heat input source term. El-Kaddah et al. (1984) make use of the Stefan results in a temperature based model to derive a one-dimensional analytical solution to the plasma spray process, and then extend the solution to reflect the two-dimensional profile of the spray front using a finite difference technique. Bewlay and Cantor (1991) use a similar finite difference formulation and incorporate contact resistance across the substrate boundary and Stefan solution profiles in the formulation for an electric spray process. Mathur et al. (1991) model the Osprey process, where a stream of previously molten metal is atomized by inert gas in a rapid solidification deposition process. The energy balance is expressed in enthalpy terms instead of temperature, as a means of handling the sharp variation of enthalpy that exists at the phase change temperature.

Existing Solidification Models

The classical consideration of a solidification (melting) front was proposed by Stefan. The original problem was intended for the prediction of the melting of sea ice and was presented as two semi-infinite surfaces (solid and liquid phases) in contact, with the contact surface defined to be at the melting temperature and the heat fluxes across this interface balanced by the release of latent heat (the Stefan condition). The analytic solution (attributed to Neumann) contains exponential and error-function terms. Crank **(1984)** provides **an in-depth review** of related Stefan formulation problems.

The bulk of the literature considering detailed treatment of a solidification front involves casting processes. As such the problems are usually stated with liquids deposited in some type of moid. A simplification often used is to assume that the liquid is at the melting temperature instead of superheated. In other formulations (Garcia and Prates, 1978; Garcia et al$_M$ 1979), the solidification of a non-superheated cast is modelled using Stefan solution approximations first with constant temperature at the mold interface and then with a semi-infinite mold model. Hills et al. (1975) include superheated liquid in a finite difference method for an unstirred mold.

Other research areas for casting problems include the consideration of natural convection effects due to the temperature induced buoyancy of the liquid phase and the finite solidification front width associated with alloys. Convection must either be included in a transfer of momentum equation, or neglected as being insignificant. Hanumanth (1990) handles this effect using finite difference methods. With the solidification of alloys there will be an intermediate "mush" region between which a fraction of the alloy metal is solid and a fraction liquid. Clyne and Kurz (1981) and Clyne (1982) present several numerical methods for the treatment of alloy solidification, as well as a method of treating this "mush" region within the heat transfer equation. Modelling the effects of convection and alloy solidification can be combined with the highly complex (and unsolved) phenomenon of dendritic growth of the solid front, as discussed by Viskanta (1988).

Existing Fluid Dynamic Models

Our current one-dimensional heat transfer modelling of **the** spray process does not require consideration of fluid dynamics. However, future efforts to

simulate the problem more accurately and for a wider range of parameters require the consideration of the hydrodynamics of the impinging droplets. Ignoring these effects is valid when the time required for **a droplet to** flatten against the substrate is significantly shorter than the time required for **the** heat transfer to occur. When the two times are of the same order of magnitude it will not be valid to ignore fluid dynamics. Hence, this flattening process is a precursor to the thermal process and may require inclusion for accurate modelling.

Direct numerical simulations involving both the hydrodynamics and temperature prediction for a droplet hitting a substrate have not been performed to date. Several models of droplet impaction have been generated to date. Madejski (1976) uses the Stefan freezing solution with total energy assumptions (kinetic, friction and surface tension terms) to derive an analytic equation for the height of a "splat". Trapaga and Szekely (1991) expand on Madejski's work by modelling the fluid dynamic effect using finite difference methods. Williams and Jones (1975) take an analytical look at the effect of the droplet temperature on the resulting thickness of the "splat". Moreau et al. (1992) investigate this problem experimentally and find that the cooling rate and the duration of the flattening process depend on substrate conditions and thickness.

Model Deficiencies

The thermal spray process to be modelled involves a liquid droplet impinging on a solid substrate, and possibly remelting a portion of **the** substrate before the entire droplet solidifies into **a "splat". The existing models outlined do** not **represent** this complete process. **The** major **drawbacks are as** follows:

1) The temperature models for spray processes do not consider the specific location of the melting front (either within the deposition layer, or with initial remelting of the substrate), and instead treat the latent heat as **an energy** input term. As an initial step in the modelling of the MD* thermal spray process, a one-dimensional heat transfer model that includes the determination of the melting front location is desired.

2) The geometry of the actual manufactured process and shape may also make the assumption of a one-dimensional problem sufficiently inaccurate for adequate temperature prediction. Depending on the orders of magnitude of the impacting and cooling processes, modelling that incorporates multi-dimensional effects, together with the dynamic effects of the droplet impaction may then be required.

3) The solidification models which typically consider alloys and casting processes do not address the physical process of superheating, rapid deposition and solidification that defines the thermal spray process. The inclusion of natural convection into the model should be unnecessary for thermal spray because there is insufficient time for this convection to develop. Alloy solidification and dendritic growth would not be required for the thermal spraying of pure metals or other non-alloy materials.

Proposed Model

The formulation of a model for determining thermal spray process temperatures is initially simplified to a purely heat transfer problem by making the assumption that an individual droplet strikes the solid surface **and flattens** much more rapidly than the time required for the droplet to solidify. **Because** the

cooling is faster than the time between droplets hitting the surface, a one droplet model is used. The shape of the impacted droplet is much wider than its height so the model can be further simplified to a one-dimensional differential equation of the form:

$$\rho^* c_p^* \frac{dT}{dt} \quad dxL \quad dxj \quad [dx^2j \quad dT \quad LdxJ \quad k \quad dx^2$$

This equation is valid for both the liquid region as well as the solid region. For the liquid region, combined convective and radiative boundary conditions exist at the top surface, while the energy balance:

$$p^*(\text{LatentHeat})^* \frac{df}{dt} = ks^* \frac{5}{dt} \text{ " } ki^* \frac{\Gamma}{dt}$$

is applied at the interface between the liquid and solid regions. For the lower boundary of the solid region a constant substrate temperature at a far distance from the spraying surface is employed (Figure 1). While the thermal conductivity (k) is a function of temperature, for the materials considered it is weakly dependent. Therefore, although the thermal property variation with temperature is modelled in the problem, the dk/dT term is not.

The above equation can then be discretized using an explicit formulation as follows:

$$ra) = r\text{-}^1(j) + a^*At/(Ax)^2*[r\text{-}^1(j+i) - 2^*r\text{-}^1(i) + r\text{-}'o\text{-}i)]$$

T"(j) is the temperature at mesh point j, and time step n

T'W) is the temperature at mesh point j, and time step n-1

$cc=k/(p^*c_p)$

The explicit form of the finite difference formulation was used because of its simplicity, however, it is then necessary to meet the stability criteria:

$$\mathbf{At} \leq \mathbf{Ax^2/(2a)}$$

The spray process is sufficiently rapid that the small time steps imposed by stability do not present a significant calculation problem.

In order to track the exact location of the melting front during the solidification process a three-point Lagrange interpolation formula is used to approximate the temperature function. This assumes a form that is similar to the above finite difference formulation, however, permits the location of a "node" point corresponding to the melting front to vary. The Lagrange formulation of the finite difference equation is used for the nodes before and after the melting point. The mesh point in the liquid region one step prior to the melting front has the formula:

$$\hat{} = 2*a/(Ax)^2*[Tmeit/(P(P+1)) - T(j)/p + p*T(j-1)/p + 1)]$$

while the mesh point in the solid region one step beyond the melting front has the formula:

$$5_{at} = 2*a/(Ax)^2*[T(j+2))/(2-p) - T(j+1)/(1-p) + T_{m8)t}/((1-p)(2-p))]$$

The parameter p has a value between 0 and 1 and represents the location of the melting front between the j and j+1 mesh points. The new value of p is calculated after each iteration using the interface energy balance equation:

$$p*(LatentHeat)*\hat{}_{at} = k.*\hat{}_{at} - ki*\frac{dT}{dt}$$

dx/dt is discretized as $(p_n - p_{n\_1})*Ax/At$

ks is the solid conductivity, k| **the** liquid conductivity.

The finite difference formulation for the latent heat energy balance equations yields:

$$p_n = P_{n-1} + c_8 * \{(2p-3) * T_m \wedge / [(1-p)(2-p)] + (2-p) * T(j+1)/(1-p) - (1-p) * T(j+2)/(2-p) - a * (p * T(j-1)/(p+1) - (p+1) * T(j)/p + (2p+1) * T_{melt}/[p(p+1)]\}$$

where $c_8 = k.*At/[p_8(LatentHeat)(Ax)^2]$

and $ci = ki*At/[p,(LatentHeat)(Ax)^2]$

For the initial interface temperature when the liquid droplet first strikes the solid substrate (with both liquid and substrate temperatures known) the Stefan interface solution is used to approximate the temperature as follows:

$$Tinter. = [RATIO * T|iq + Tsol]/[1 + RATIO\,1$$

$$RATIO = [(k * c_p * p)_{liq}/(k * Cp * p)_{8Ol}]^{1/2}$$

For the complete duration of the thermal spray system modelling, the Stefan solution is not an accurate representation of the actual boundary conditions. However, for the initial interface condition the solution above can be used because boundary conditions corresponding to two semi-infinite bodies in contact do remain valid until the temperature propagates to the liquid surface.

Results

The model described above has been implemented for the cases of a 304 stainless steel droplet on a similar substrate, a zinc droplet on a zinc substrate, and a stainless steel droplet on a zinc substrate. The importance of model-related effects of spatial and temporal resolution are investigated, as well as the

effect that the surface convection/radiation conditions have on the results. The primary focus of the simulation then involves the effect that the droplet size and temperature has on the remelting phenomenon, and similarly the effect that substrate temperature has on the remelting.

For a given model, the size of the liquid droplet is required as input. The discretization is then performed to fix the ratio of the mesh points spanning the liquid and solid regions. To ensure the validity of the lower boundary condition (Too equals initial Tsub), simulations were run where the ratio of liquid to solid was chosen to create a very large solid region (Figure 2). Based on the results, a minimum substrate depth of 750 microns was required for a liquid droplet size of 100 microns to ensure that the lower boundary condition remains valid during the time of the simulation. This mesh size and ratio is then used for all simulations.

Both spatial and temporal resolution are investigated. For a 100 micron droplet, it is necessary to divide the droplet into 20 nodes to converge on a solution; further subdivision only increased computation time without any change of accuracy. While the numerical stability criterion (previously stated) imposes a maximum time step of less than $3x10^{-7}$ seconds, the solution converges when step sizes were less than $5x10^{-9}$ (Figure 3). This additional time step refinement is probably influenced by the added approximation introduced by the Lagrange temperature interpolation used to resolve the melting front migration.

The surface convection and radiation effects are also analyzed by performing a sensitivity analysis of the convection and radiation parameters. The surface heat transfer coefficient is calculated using a correlation for impinging gas forced convection (Guyer, 1989). The radiation is considered to be a constant input source resulting from the plasma nozzle (Pawbwski et al., 1981).

Both of these effects are found to be insignificant compared to the conduction of heat into the substrate. The conclusion is that the conduction is such a rapid effect that convection/radiation effects do not have sufficient time to take place.

For both the cases of stainless steel impinging on stainless steel and zinc impinging on zinc, the initial conditions are varied in an attempt to achieve remelting. For stainless steel, Figure 3 shows the effect of increasing droplet temperature on remelting, Figure 4 the effect of increased droplet size on remelting, and Figure 5 the effect of increased substrate temperature. Figures 6 through 8 show similar effects for zinc.

The conclusions drawn are that remelting will not occur for "reasonable" droplet temperatures without significant substrate heating above ambient temperatures. This can be influenced by either directly pre-heating the substrate, or by controlling the rate of spraying, the temperature of the impinging droplets, and the cooling rate of the substrate. Because zinc has a higher thermal diffusivity, it is more readily remelted than stainless steel. A reasonable temperature is considered to be only a few hundred degrees above the melting point (1425°C for stainless steel, 420°C for zinc). Increasing the droplet size extends the time for solidification to occur and increases the thickness of remelting (when conditions permit remelting), but it does not create a remelting condition if the temperatures are insufficient.

For the simulation of a stainless steel droplet impinging on a zinc substrate the melting point of the stainless steel is sufficiently high enough to generate melting in the zinc regardless of droplet size. For larger droplet sizes, the extent of remelting increases. Again, with its greater thermal diffusivity, the layer of zinc remelted is larger than the stainless steel droplet size. This model actually tracks

two simultaneous melting fronts, because while the zinc is melting, the stainless steel is solidifying. This model offers a more qualitative simulation of the two-metal phenomenon because the model temperatures at the interface indicate that a small (20 micron) layer of the zinc exceeds the zinc boiling point, while the model does not account for the heat of vaporization that would accompany this phase change.

Future Activities

Thermal spraying is a very complex process that has tended to develop and evolve in an empirical fashion. For this reason, and the fact that any mathematical model must be verified, it will be necessary to compare model results with actual data. Knowledge of the actual spraying temperatures experienced are required to verify that electronic components will not be damaged. This can be accomplished using thermocouples sprayed or embedded in the test monolith. The determination of a remelting condition, which takes place in an order of magnitude of 10^{-3} seconds, can be verified using metallographic examinations. Metallographic techniques are expected to yield information not only on the extent of remelting (depth) but also the rate of cooling, as reflected by the resulting microstructure (McPherson, 1981).

It will be necessary to measure the resulting thermal properties of various sprayed materials at varying operating conditions so as to correlate spray parameters with resulting material properties. There is also a need to extend the modelling to include the fluid dynamic effects of droplet impact and the two-dimensional effect of lateral heat transfer.

References

1. Bewlay, B.P., and Cantor, B., 1991, The Relationship Between Thermal History and Microstructure in Spray-Deposited Tin-Lead Alloys," *J. of Mat. Res.,* Vol. 6, No. 7, pp. 1433-1454.

2. Clyne, T.W., and Kurz, W., 1981, "Solute Redistribution During Solidification with Rapid Solid State Diffusion," *Metall. Trans. A,* 12A, pp. 965-971.

3. Clyne, T.W., 1982, "Numerical Modelling of Directional Solidification of Metallic Alloys," *Metal Science,* Vol. 16, pp. 441-450.

4. Crank, J., 1984, Free and Moving Boundary Problems, Oxford Press, New York.

5. El-Kaddah, N., McKelliget, J., and Szekely, J., 1984, "Heat Transfer and Fluid Flow in Plasma Spraying," *Metall. Trans. B,* 15B, pp. 59-70.

6. Garcia, A., and Prates, M., 1978, "Mathematical Model for the Unidirectional Solidification of Metals: I. Cooled Molds," *Metall. Trans. B,* 9B, pp. 449-457.

7. Garcia, A., Clyne, T.W., and Prates, M., 1979, "Mathematical Model for the Unidirectional Solidification of Metals: II. Massive Molds," *Metall. Trans. B,* 10B, pp. 85-92.

8. Gerdeman, D.A., and Hecht, N.L, 1972, Arc Plasma Technology in Materials Science, Springer-Verlag, New York.

9. Guyer, E.C., ed., 1989, Handbook of Applied Thermal Design, McGraw-Hill, New York.

10. Hanumanth, G.S., 1990, "Solidification in the Presence of Natural Convection," *Int. Comm. Heat Mass Transfer,* Vol. 17, pp. 283-292.

11. Hills, A.W.D., Malhotra, S.L, and Moore, M.R., 1975, "The Solidification of Pure Metals (and Eutectics) Under Unidirectional Heat Flow Conditions: II. Solidification in the Presence of Superheat," *Metal. Trans. B,* 6B, pp. 131-142.

12. Madejski, J., 1976, "Solidification of Droplets on a Cold Surface," *Int. J. Heat Mass Transfer,* Vol. 19, pp. 1009-1013.

13. Mathur, P., Apelian, D., and Lawley, A., 1989, "Analysis of the Spray Deposition Process," *Ada Metallica,* Vol. 37, No. 2, pp. 429-443.

14. McPherson, R., 1981, "The Relationship Between the Mechanism of Formation, Microstructure and Properties of Plasma Sprayed Coatings," *Thin Solid Films,* Vol. 83, pp. 297-310.

15. Moreau, C, Cielo, P., and Lamontagne, M., 1992, "Flattening and Solidification of Thermal Sprayed Particles," *Proc. Int. Thermal Spray Conf.,* pp. 761-766.

16. Pawlowski, L., Vardelle, M., and Fauchais, P., 1981, Temperature Distribution in Plasma-Sprayed Coatings," *Thin Solid Films,* Vol. 81, pp. 79-88.

17. Pawlowski, L, 1982, "A Model of the Temperature Distribution in an Alumina Coating During Plasma-Spray," *Thin Solid Films,* Vol. 94, pp. 307-319.

18. Szekely, J., and Jassal, A.S., 1978, "An Experimental and Analytical Study of the Solidification of a Binary Dendritic System," *Metall. Trans. B,* 9B, pp. 389-398.

19. Trapaga, G., and Szekely, J., 1991, "Mathematical Modelling of the Isothermal Impingement of Liquid Droplets in Spraying Processes," *Metall. Trans. B,* 22B, pp. 901-914.

20. Viskanta, R., 1988, "Heat Transfer During Melting and Solidification of Metals," *J. Heat Transfer,* Vol. 110, pp. 1205-1219.

21. Weiss, L.E., Prinz, F.B., Adams, D.A., and Siewiorek, D.P., 1992, "Thermal Spray Shape Deposition," *J. Thermal Spray Technology,* Vol. 1(3), pp. 231-237.

22. Williams, C.A., and Jones, H., 1975, The Effect of Melt Superheat and Impact Velocity on Splat Thickness," *Materials Science and Engineering,* Vol. 19, pp. 293-297.

Figure Captions

Figure 1. "Model Formulation/ Overview of the model boundary conditions and melting front movement.

Figure 2. "Temperature vs. Time," Results from the simulation using zinc, with an extended solid region.

Figure 3. "Temporal Stability," Melting front location vs. time using zinc, for various time step increments.

Figure 4. "Melting Front Migration," 304 stainless steel with a constant substrate temperature and droplet size, and varied droplet temperature.

Figure 5. "Drop Size Effect,* 304 stainless steel with a constant substrate temperature and droplet temperature, and varied droplet size.

Figure 6. "Melting Front Migration," 304 stainless steel with a constant droplet temperature and droplet size, and varied substrate temperature.

Figure 7. "Droplet Temperature Effects," Zinc with a constant substrate temperature and droplet size, and varied droplet temperature.

Figure 8. "Drop Size Effect" Zinc with a constant substrate temperature and droplet temperature, and varied droplet size.

Figure 9. "Substrate Temperature Effects," Zinc with a constant droplet size and droplet temperature, and varied substrate temperature.

Figure 10. "Melting Front Migration," Stainless steel droplet on zinc substrate. Droplet size and substrate temperature constant, droplet temperature varied.

Figure 11. "Melting Front Migration," Stainless steel droplet on zinc substrate. Droplet temperature and substrate temperature constant, droplet size varied.

Model Formulation
(Figure 1)

Tllq

(8»ll«lfleatio$_a$ fmat)

t p _ _ _ _

TlnIt

Taol

- Surface B.C.:
  Conduction and Radiation
- Tin it calculated
  by Stefan approx.
- Interface B.C.:
  Energy balance with
  latent heat release
- Bottom B.C.:
  Constant temperature

Temperature vs. Time
(Figure 2)

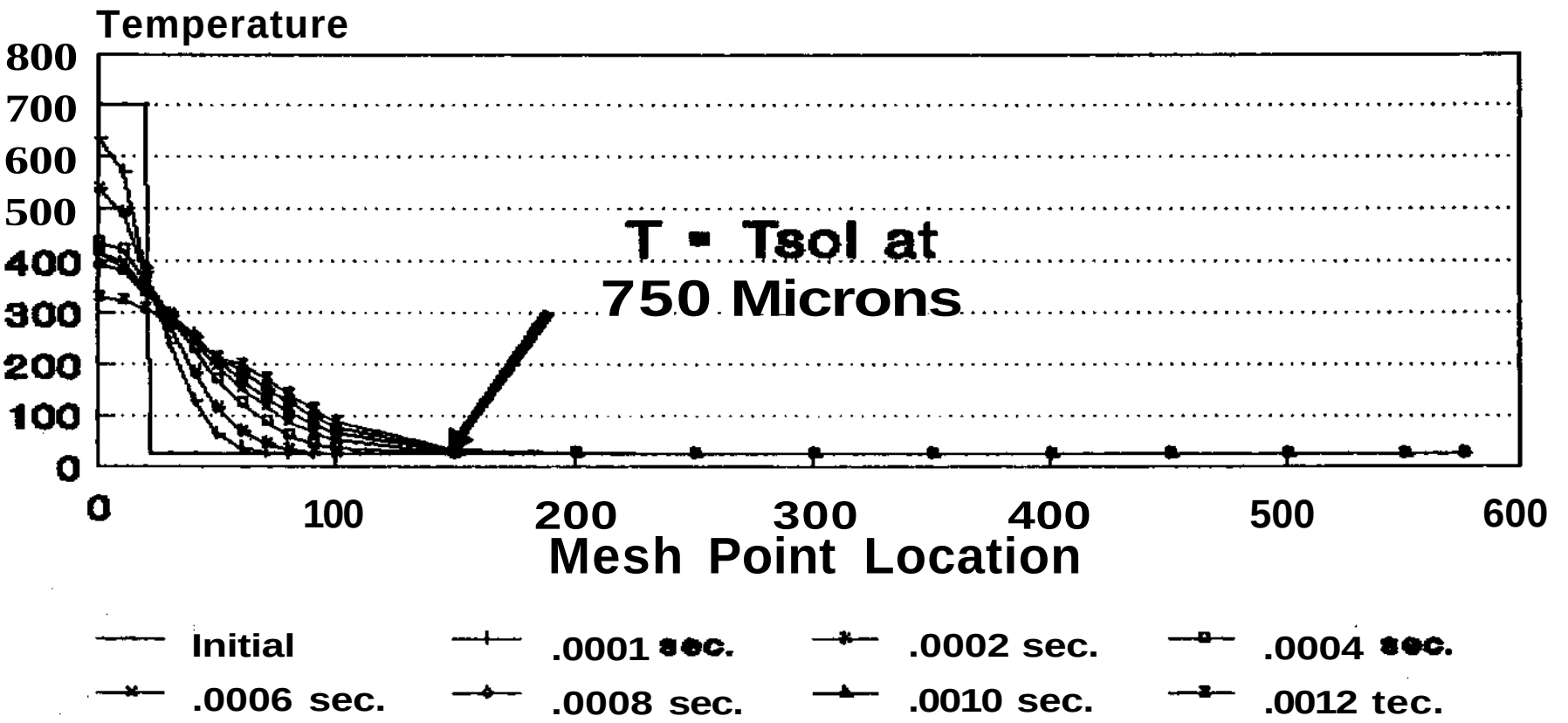

(Zinc w/ Tllq - 700
Teub - 26. d - 100}

TEMPORAL STABILITY
(Figure 3)

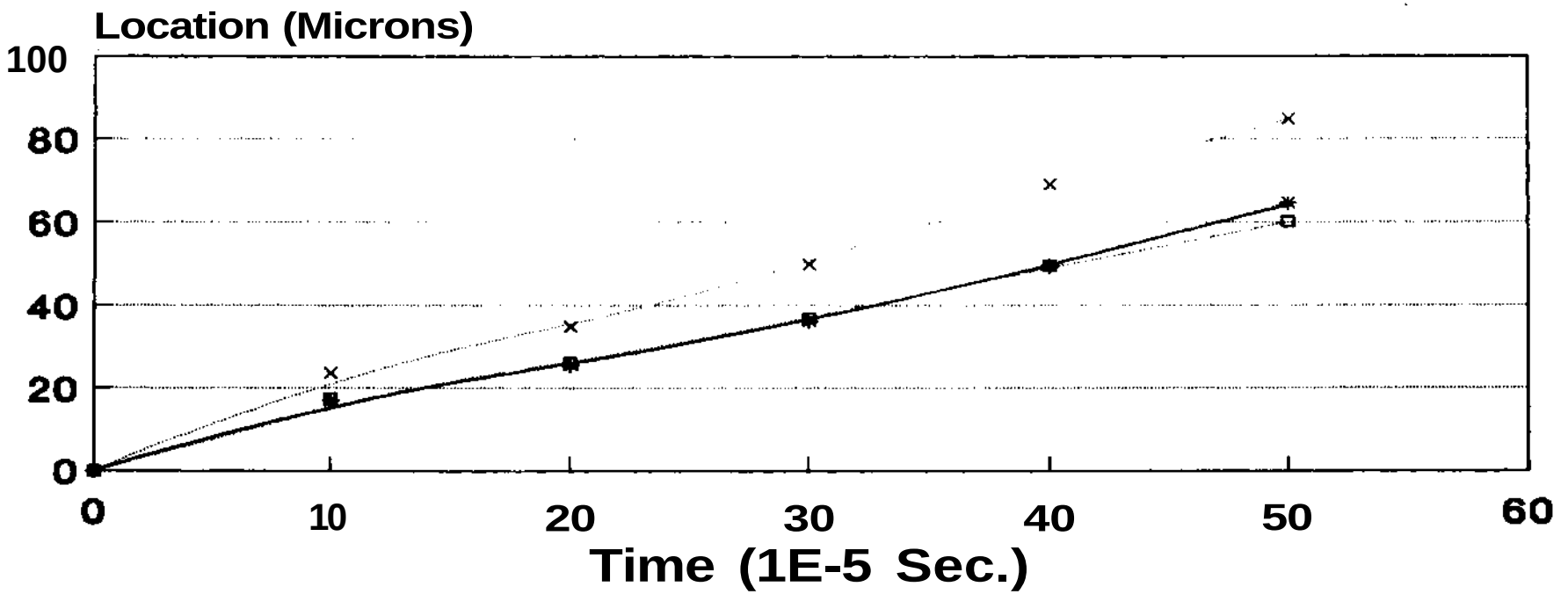

(Zinc w/ Tliq - 700, Tsub - 25, d - 100)

(Stability Calc. - 3E-7 sec.)

Melting Front Migration
(Figure 4)

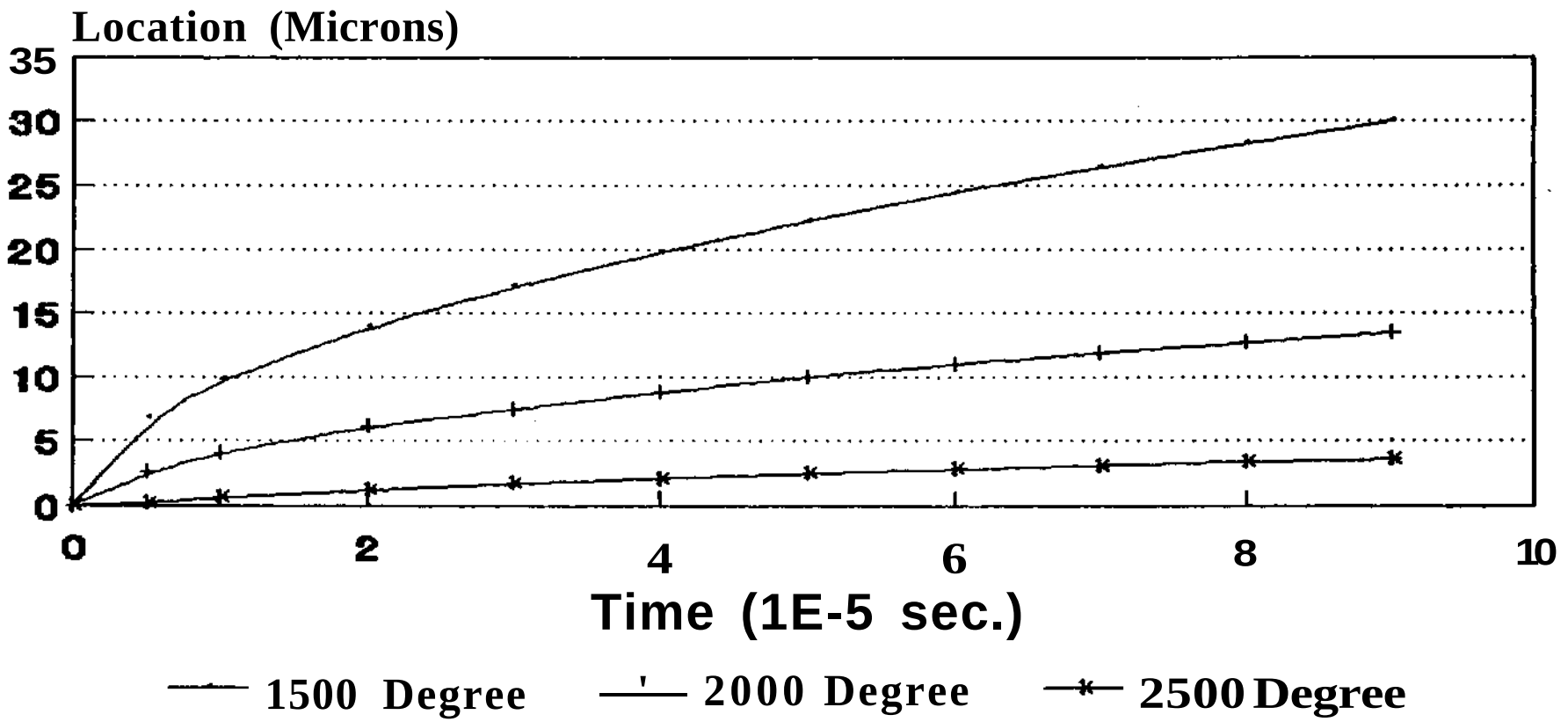

(304 Stainless Steel.
Tsub - 100.
Drop size - 100 microns)

DROP SIZE EFFECT
(Figure 5)

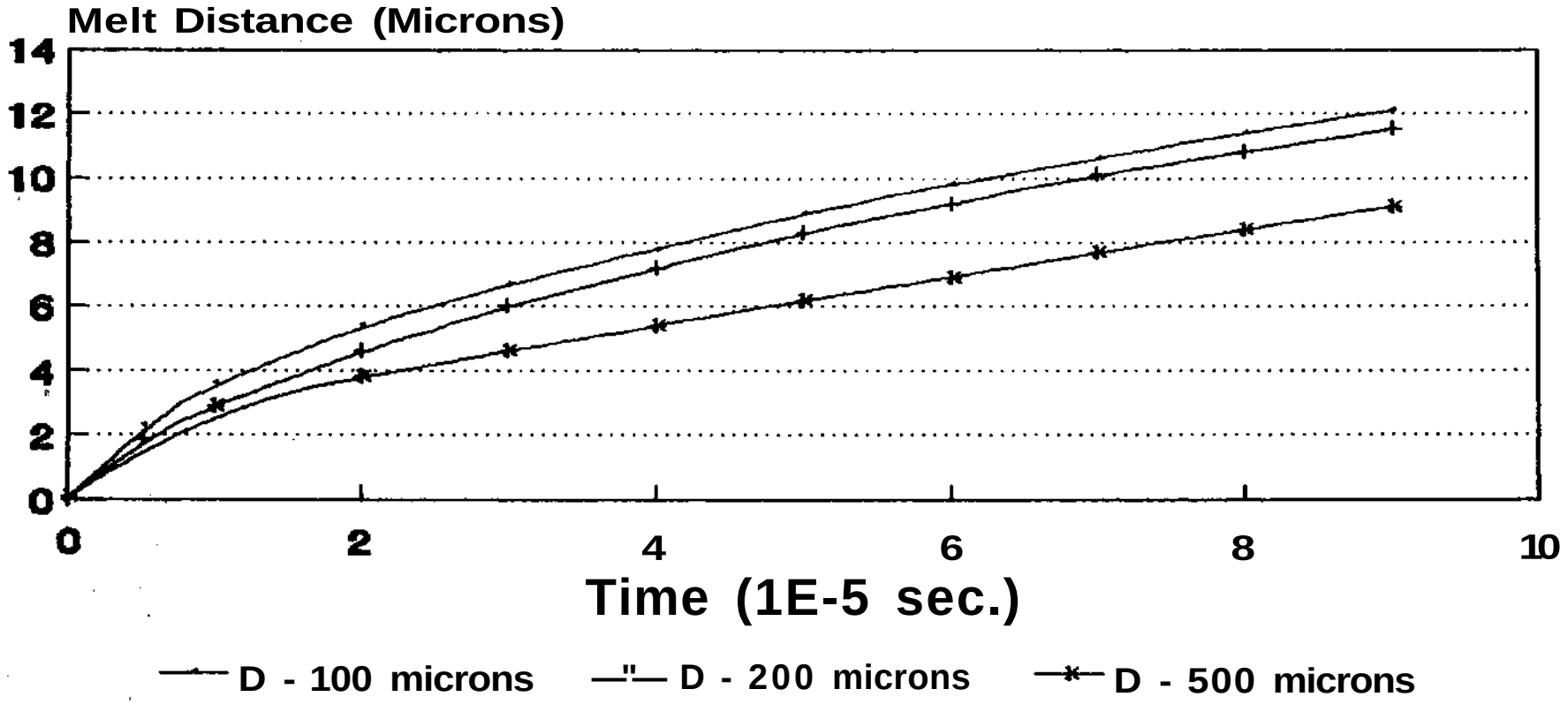

(Stainless Steel.
Tllq - 2000.
fsub -200)

Melting Front Migration
(Figure 6)

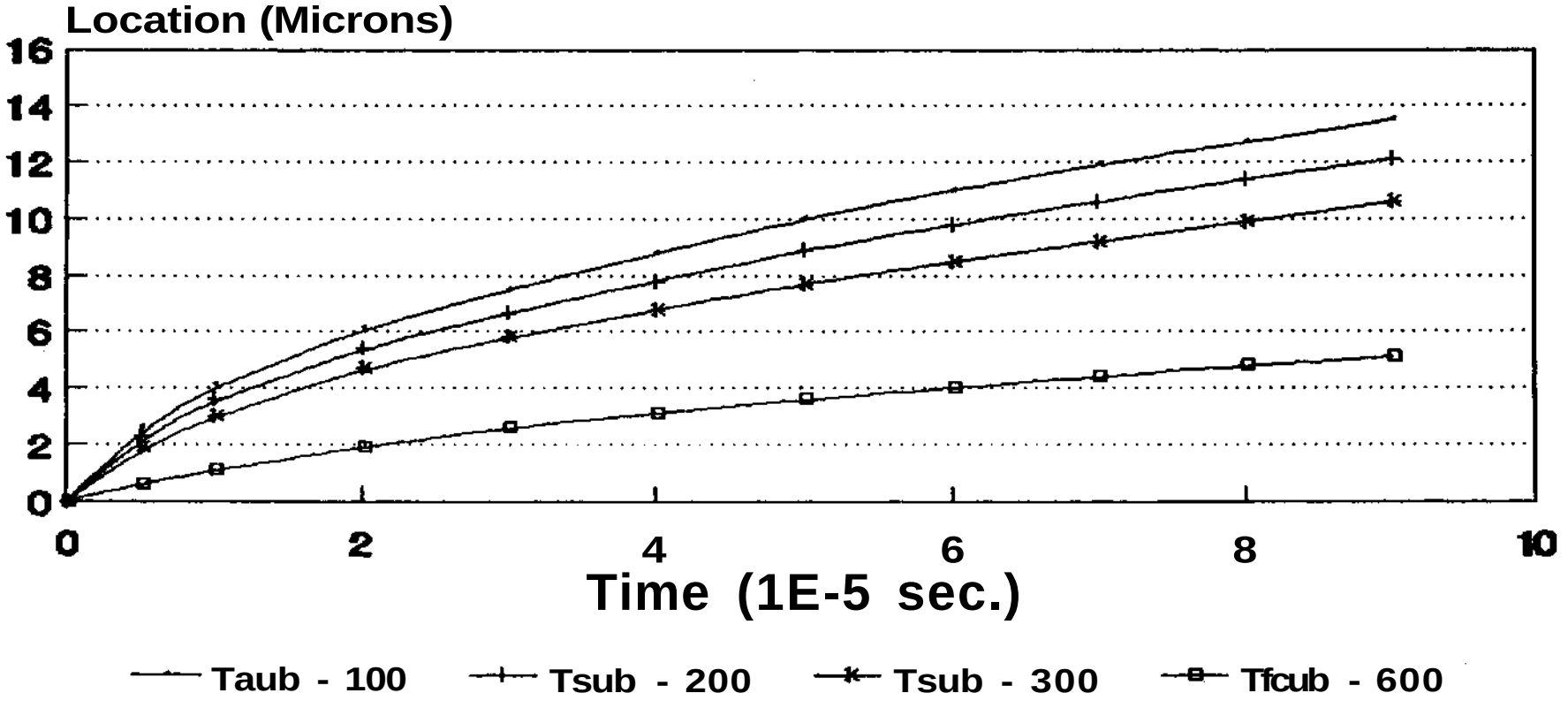

(304 Stainless Steel.
Tllq - 2000.
Drop size - 100 microns)

Droplet Temperature Effects
(Figure 7)

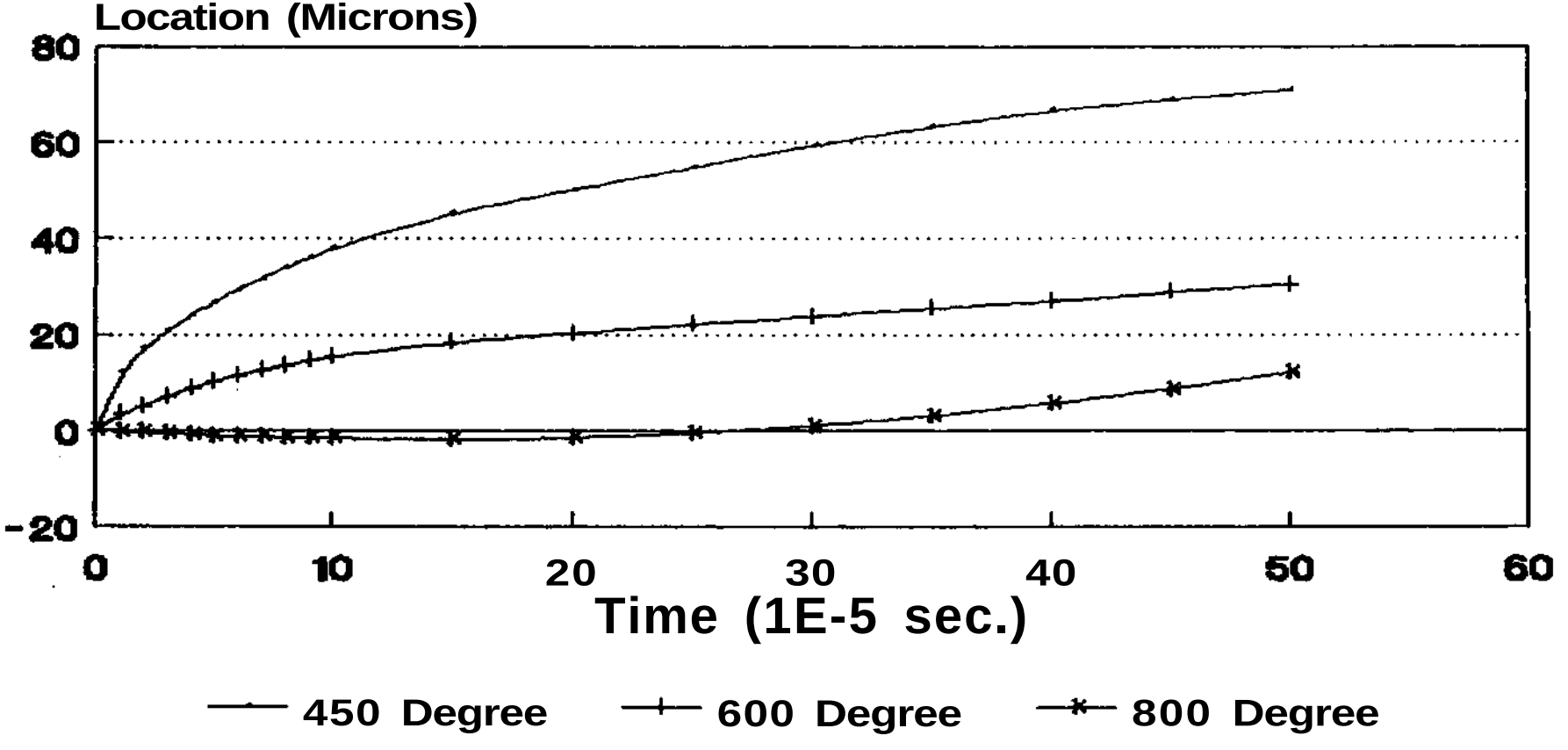

:Zfno w/ T«ub - 25.
drop - 100 microns)

DROP SIZE EFFECT
(Figure 8)

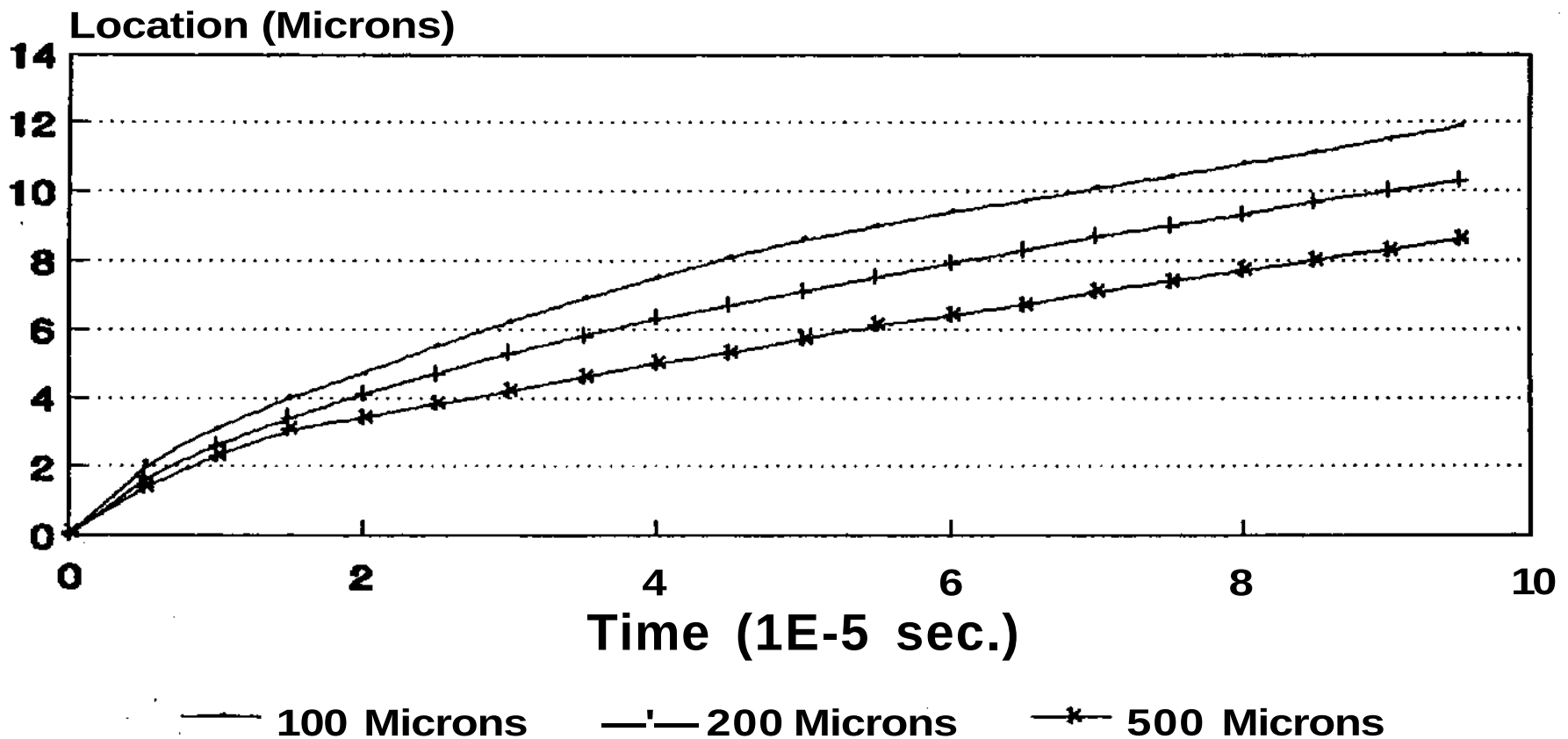

(Zinc Tllq - 600.
Tsub - 100)

Substrate Temp. Effects
(Figure 9)

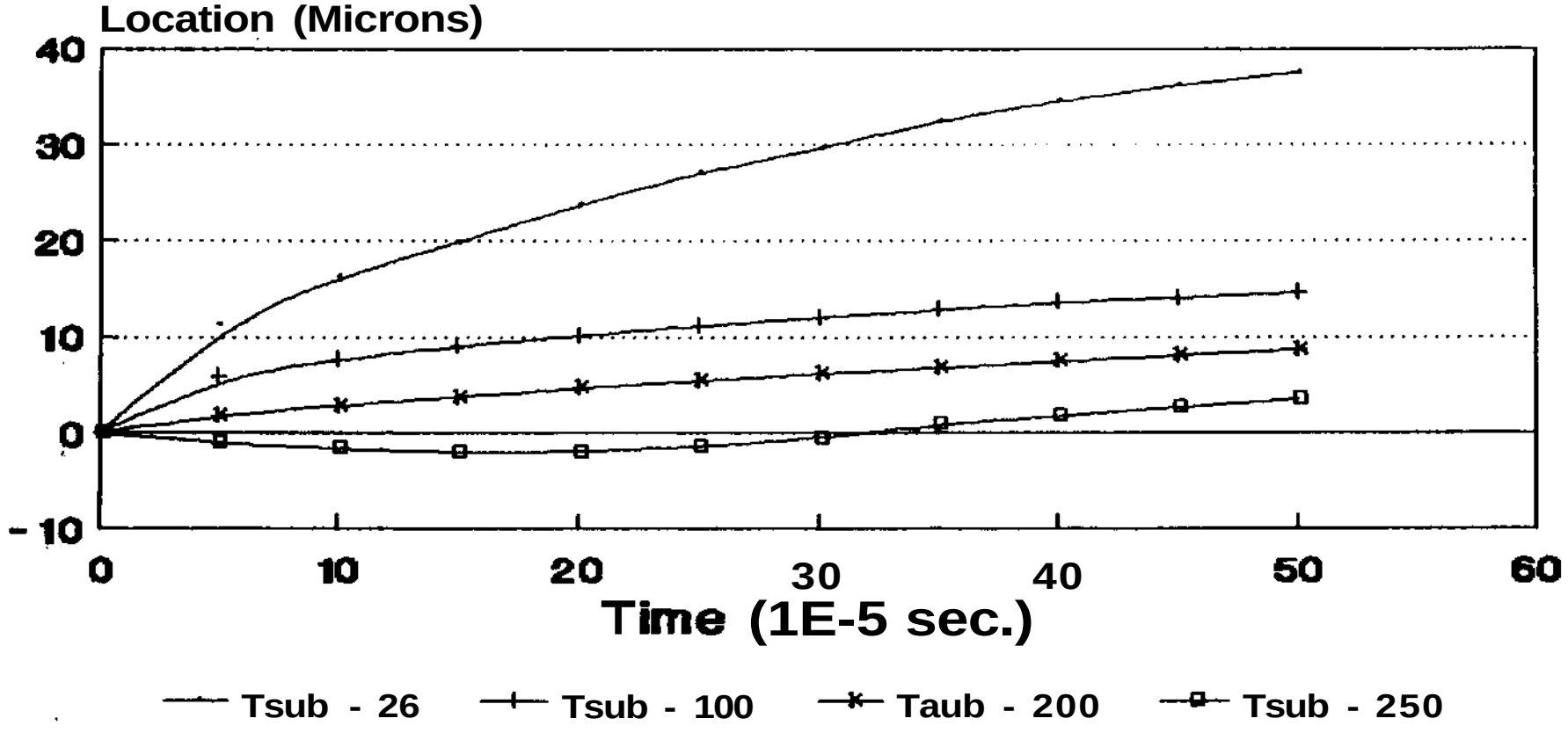

(Zinc w/ Tliq - 600.
drop - 100 microns

Melting Front Migration
(Figure 1O)

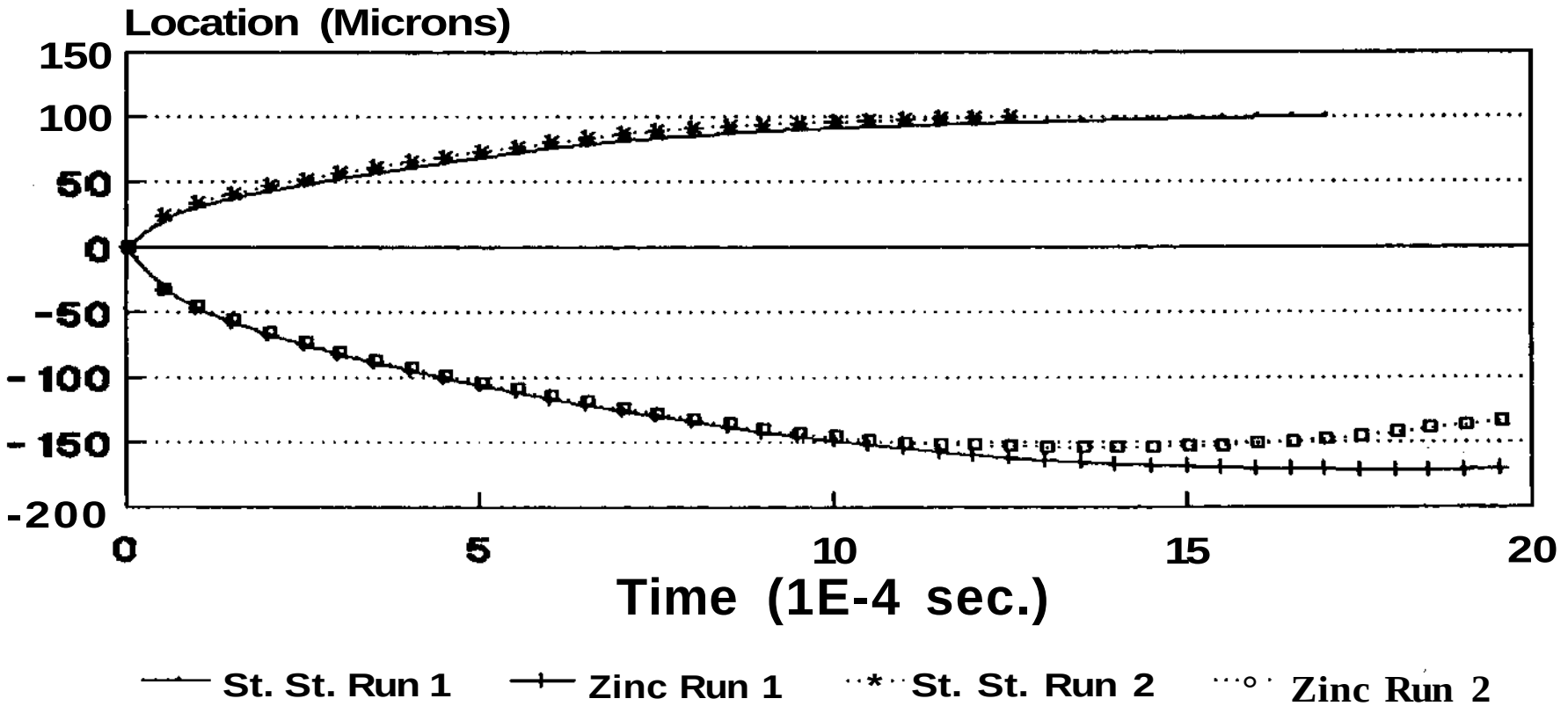

(Stainless Steel on Zinc substrate.
Tsub - 25. drop - 100 microns.
Tllq for: Run 1 - 1600. Run 2 - 1450)

Melting Front Migration
(Figure 11)

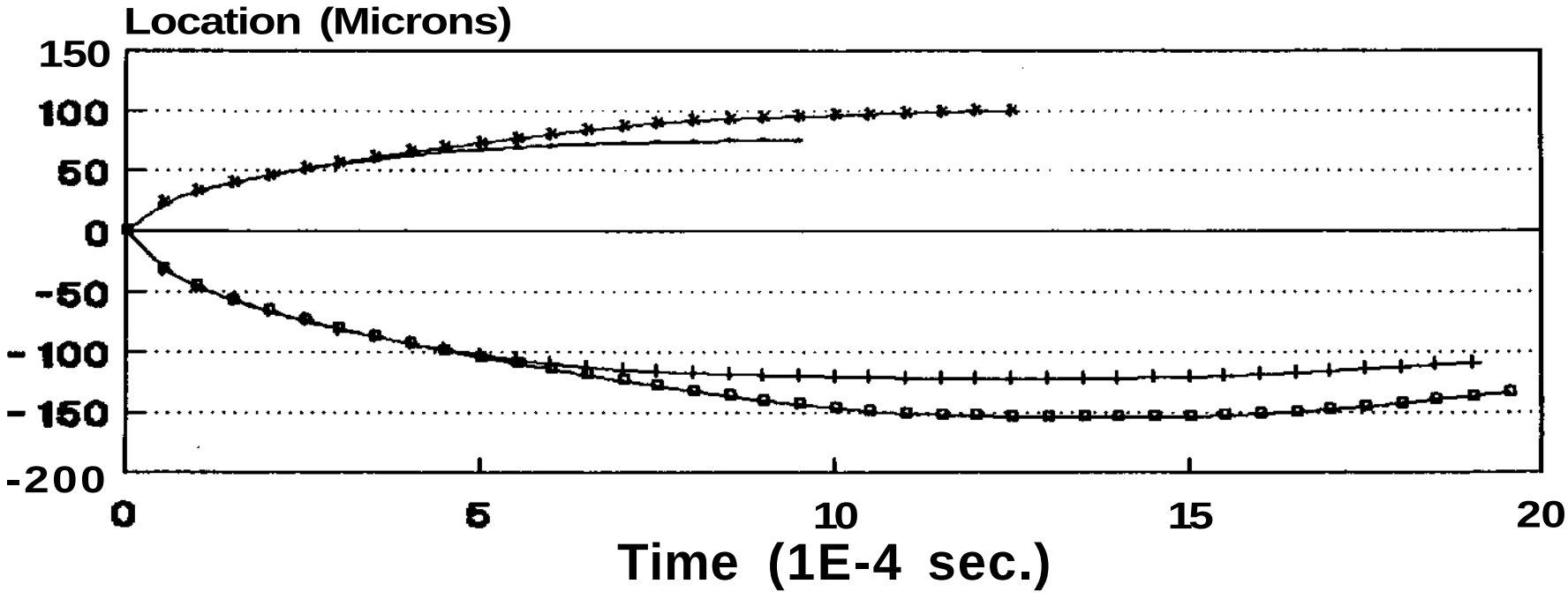

(Stalnleaa Steel on Zinc **substrate.**
Tllq - 1450. Taub - 25)